Chemical Science

ROYAL SOCIETY OF CHEMISTRY

PERSPECTIVE

View Article Online
View Journal | View Issue

Cite this: *Chem. Sci.*, 2023, **14**, 9248

All publication charges for this article have been paid for by the Royal Society of Chemistry

Received 23rd June 2023
Accepted 27th July 2023

DOI: 10.1039/d3sc03198e

rsc.li/chemical-science

Transition-metal (oxy)nitride photocatalysts for water splitting

Kaihong Chen, [a] Jiadong Xiao, [a] Takashi Hisatomi [ab] and Kazunari Domen *[acd]

Solar-driven water splitting based on particulate semiconductor materials is studied as a technology for green hydrogen production. Transition-metal (oxy)nitride photocatalysts are promising materials for overall water splitting (OWS) *via* a one- or two-step excitation process because their band structure is suitable for water splitting under visible light. Yet, these materials suffer from low solar-to-hydrogen energy conversion efficiency (STH), mainly because of their high defect density, low charge separation and migration efficiency, sluggish surface redox reactions, and/or side reactions. Their poor thermal stability in air and under the harsh nitridation conditions required to synthesize these materials makes further material improvements difficult. Here, we review key challenges in the two different OWS systems and highlight some strategies recently identified as promising for improving photocatalytic activity. Finally, we discuss opportunities and challenges facing the future development of transition-metal (oxy)nitride-based OWS systems.

Introduction

The conversion of solar energy into chemical fuels is an intriguing approach to alleviating energy and environmental issues. Given the high gravimetric energy density of hydrogen (H_2), solar-driven overall water splitting (OWS) into H_2 and oxygen (O_2) offers a possibility to take full advantage of solar energy.[1] To date, an apparent quantum yield (AQY) of almost unity has been achieved in OWS using an Al-doped $SrTiO_3$ particulate photocatalyst facet-selectively modified with Rh/

[a]*Research Initiative for Supra-Materials, Interdisciplinary Cluster for Cutting Edge Research, Shinshu University, Nagano-shi, Nagano 380-8553, Japan. E-mail: domen@shinshu-u.ac.jp*

[b]*PRESTO, JST, 4-17-1 Wakasato, Nagano-shi, Nagano 380-8553, Japan*

[c]*Office of University Professors, The University of Tokyo, 2-11-16 Yayoi, Bunkyo-ku, Tokyo 113-8656, Japan*

[d]*Department of Chemistry, Kyung Hee University, Seoul 130-701, Republic of Korea*

Kaihong Chen obtained his PhD in chemistry (2018) at Zhejiang University under the supervision of Prof. Congmin Wang. He then pursued his postdoctoral research with Prof. Liangnian He at Nankai University. From August 2021, he worked as a JSPS postdoctoral fellow with Prof. Kazunari Domen at Shinshu University. Now, he works in the Institute of Green Chemistry and Engineering at Nanjing University. His current research interests are photocatalytic water splitting and CO_2 utilization.

Jiadong Xiao obtained a PhD in engineering at the University of the Chinese Academy of Sciences under Prof. Hongbin Cao's supervision in 2018 and performed PhD exchange studies at the Leibniz Institute for Catalysis under Prof. Angelika Brückner's supervision from 2016 to 2018. He worked as a postdoctoral researcher at Utrecht University with Prof. Bert M. Weckhuysen in 2018 and 2019. Since then, he has joined Prof. Kazunari Domen's laboratory as a postdoctoral researcher and was promoted to specially appointed assistant professor at Shinshu University in 2022. His main research interests include (photo)catalysis for sustainability and (photo)catalytic in situ/operando studies.

Cr_2O_3 and CoOOH cocatalysts *via* photodeposition.[2] Even so, the solar-to-hydrogen energy conversion efficiency (STH) of this system is only 0.65% because Al-doped $SrTiO_3$ responds solely to ultraviolet light. The STH value necessary to make this process economically competitive with H_2 production from fossil resources has been estimated to be approximately 5–10%.[3] Clearly, it is necessary to develop narrow-bandgap photocatalysts that have a longer absorption-edge wavelength to effective utilize visible components in sunlight.[4,5]

Compared with metal oxide semiconductors, (oxy)nitride semiconductors have narrower bandgaps because N 2p orbitals have a more negative potential energy than O 2p orbitals and because the valence-band edge is shifted negatively.[6] As a result, the absorption edges of these (oxy)nitride materials are mostly extended to the visible-light range while band-edge potentials suitable for OWS are maintained.[7–10] For instance, with increasing N content, the absorption-edge wavelengths become longer: from ~320 nm for Ta_2O_5 to ~500 nm for TaON and ~600 nm for Ta_3N_5. Thermodynamically, all of these materials can evolve both H_2 and O_2 from an aqueous solution.[11] Note that nitrogen-doped transition-metal oxides have been reviewed elsewhere[12,13] and will not be discussed in this perspective, because N atoms only form impurity (discontinuous) levels in these materials.

Apart from the extension of the absorption edge, charge separation and migration should also be improved and the desired surface redox reactions should be enhanced to increase the OWS activity.[11] However, the situation is complicated and often difficult to control when transition-metal (oxy)nitride-based photocatalysts are used. First, anion vacancies and reduced species (*e.g.*, $Ta^{4+/3+}$ or Ti^{3+}) are inevitably formed during high-temperature nitridation under flowing ammonia (NH_3) because of the decomposition of NH_3 into N_2 and H_2 at high temperatures. Such defects can function as recombination centers, decreasing the number of surviving photoexcited charge carriers and reducing the photocatalytic activity. In addition, a complicated nitridation process (anion exchange and rearrangement) also limits the availability of (oxy)nitrides with well-defined facets. Moreover, the poor thermal stability of (oxy)nitrides at elevated temperatures in air is a large obstacle to the design of effective cocatalyst loading procedures. Even though most oxynitride materials are expensive, the material cost of the photocatalyst is estimated to be insignificant compared with the cost of the photocatalytic reactor due to the small amount of the photocatalyst loaded, and therefore will be allowable.[3]

Numerous transition-metal (oxy)nitrides have been shown to exhibit activities toward both the H_2 evolution reaction (HER) and the O_2 evolution reaction (OER) in the presence of sacrificial electron donors and acceptors, respectively.[7] However, very few of them have shown activity in the one-step-excitation or two-step-excitation (*i.e.*, Z-scheme process) OWS reaction. In addition, in the few known cases of OWS-active transition-metal (oxy)nitride photocatalysts, the AQY is relatively low. For example, a $BaTaO_2N$-based photocatalyst with a bandgap of 1.9 eV was recently reported to achieve OWS *via* one-step excitation; however, the AQY was less than 0.1% at 420 nm.[14] In fact, the STH value for an OWS process driven solely by (oxy)nitrides has not exceeded 0.3% yet, irrespective of whether one-step or two-step excitation systems are used. This poor photocatalytic performance is partially attributable to the surface reduction or oxidation reactions being much more sluggish in the absence of sacrificial reagents, which allows unreacted electrons and holes to simply recombine.

The development of strategies that can increase the STH value for OWS using (oxy)nitride photocatalysts is critical and urgently needed. In this perspective, we summarize some key strategies developed for enhancing OWS activity by one- or two-step excitation schemes using transition-metal (oxy)nitride photocatalysts. Our goal is to provide a springboard for further research.

Takashi Hisatomi received a PhD in engineering from the University of Tokyo in March 2010. He worked as a post-doctoral fellow in École Polytechnique Fédérale de Lausanne from April 2010 to March 2012. He moved to the University of Tokyo in April 2012 as a post-doctoral fellow and acquired an assistant professor position in August 2012. He moved to Shinshu University as an associate professor in April 2018 and was promoted to professor in April 2023. His major research interests include semiconductor photocatalysts for overall water splitting, kinetics of photoexcited carriers in semiconductors, and reaction systems for renewable solar hydrogen production.

Kazunari Domen is a special contract professor at Shinshu University and university professor at the University of Tokyo, Japan. He received a PhD in science from the University of Tokyo in 1982. He joined the Tokyo Institute of Technology in 1982 as an assistant professor and was promoted to associate professor in 1990 and professor in 1996. He moved to the University of Tokyo as a professor in 2004 and was appointed by Shinshu University as a special contract professor in 2017. His research interests include heterogeneous catalysis and materials chemistry, with a particular focus on photocatalytic water splitting for solar hydrogen production.

Two OWS systems

Before describing challenges and strategies for enhancing the OWS activity of photocatalytic systems based on transition-metal (oxy)nitrides, basic aspects of one- and two-step-excitation OWS systems are introduced because the reaction properties required for the respective systems differ. The one-step-excitation OWS reaction has been studied intensively for decades as a simple and readily scaled-up approach.[15–18] In this scheme, the bandgap of the semiconductor photocatalyst should straddle both the HER and OER potentials (Fig. 1a). In addition, because the HER and OER occur on the same photocatalyst, the photocatalysts need to be carefully designed to promote spatial charge separation and HER/OER processes while suppressing the water-formation reaction. To this end, in most cases, several strategies are applied concurrently to realize the one-step-excitation OWS reaction.

Inspired by natural photosynthesis, a typical Z-scheme OWS system comprises a H_2-evolution photocatalyst (HEP), an O_2-evolution photocatalyst (OEP), and shuttle redox mediators.[19,20] As shown in Fig. 1b, the HEP and OEP produce H_2 and O_2 separately and the redox mediator functions as an electron mediator between the HEP and OEP. Photocatalysts can be used in Z-scheme OWS as long as they are active either toward the HER or the OER; therefore, the bandgap of the photocatalyst is not required to straddle both the HER and OER potentials. This approach provides opportunities for narrow-bandgap photocatalysts to participate in OWS under visible light. However, this feature utilizing a cascade of electron flow also provides opportunities for backward electron transfer. Undesirable backward reactions involving redox couples, in addition to those involving the water-formation reaction, should therefore be suppressed.

Z-scheme OWS systems

We first describe progress and challenges associated with Z-scheme OWS despite the complexity of the system, because many strategies originally developed to promote half-reactions have been effectively exploited for Z-scheme OWS prior to the realization of one-step-excitation water splitting. In this section, we highlight some representative strategies such as reducing defect densities, promoting charge separation and migration, and loading cocatalysts to promote surface redox reactions.

Reduction of defect densities

The synthesis of (oxy)nitrides by NH_3 nitridation at high temperature tends to generate defects both in the bulk and at the surface. Decreasing the defect density is an important target for transition-metal (oxy)nitrides used in OWS. One reason for the formation of defects is the structure difference between the precursors and the target products. In this context, a radical redesign of the starting materials and synthesis procedure could be beneficial. Xu *et al.* designed some double-layer Sillén–Aurivillius-type compounds, in which the Aurivillius units contain perovskite-type blocks topotactically similar to (oxy)nitrides (Fig. 2a), as precursors.[21–23] $(Bi_{0.75}La_{0.25})_4TaO_8Cl$ can be transformed into $LaTaO_2N$ (denoted as $LaTaO_2N$-P) under high-temperature nitridation.[21] During the nitridation, Bi^{3+} and Cl^- ions evaporate and the residual perovskite-type blocks are converted to $LaTaO_2N$ without a drastic rearrangement of the atoms. Meanwhile, the evaporation of Bi^{3+} and Cl^- ions can form voids in the particles to facilitate replacement of O by N, which helps suppress the reduction of Ta^{5+} (Fig. 2b).[21] After CoO_x was loaded as an O_2-evolution cocatalyst (OEC), the OER activity of such porous $LaTaO_2N$ was six times greater than that of $LaTaO_2N$ prepared from $LaTaO_4$. When combined with a Ru/$SrTiO_3$:Rh HEP and a Fe^{3+}/Fe^{2+} redox mediator, the porous $LaTaO_2N$ could split water under visible light *via* the Z-scheme.

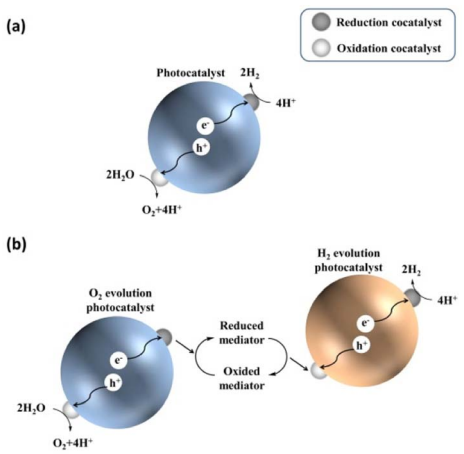

Fig. 1 Schematics of (a) one-step-excitation and (b) two-step-excitation (Z-scheme) overall water-splitting processes.

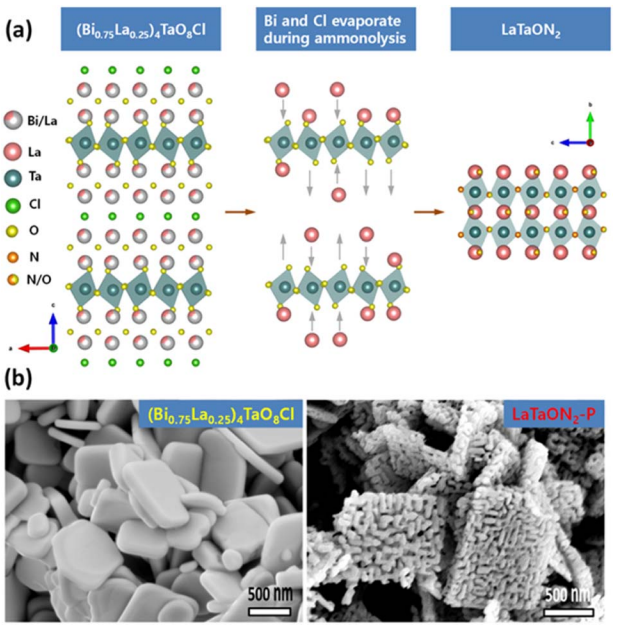

Fig. 2 (a) Schematic of structural transformation from $(Bi_{0.75}La_{0.25})_4TaO_8Cl$ into $LaTaO_2N$. (b) Field-emission scanning electron microscopy images of $(Bi_{0.75}La_{0.25})_4TaO_8Cl$ and $LaTaON_2$-P. Adapted with permission from ref. 21. Copyright 2021 American Chemical Society.

Moreover, this topotactic conversion strategy has been extended to the synthesis of $SrTaO_2N$ and $SrNbO_2N$.[22,23]

The addition of certain additives to precursors can also afford the desired transition-metal (oxy)nitride photocatalysts. Recently, the flux-assisted nitridation technique has emerged as a powerful method to prepare (oxy)nitrides with controllable crystallinity, morphology, surface features, and particle size. Li *et al.* discovered that $BaTaO_2N$ prepared *via* a flux method exhibits weaker background absorption in the 700–800 nm range, indicating a decreased defect density compared with $BaTaO_2N$ nitrided in the absence of a flux.[24] Using a $LiBa_4Ta_3O_{12}$ oxysalt as a precursor, in which the Li^+ was easily evaporated, they fabricated $BaTaO_2N$ (denoted as $BaTaO_2N$-flux) with a porous structure and low defect density.[24] A Z-scheme OWS reaction using the Pt/$BaTaO_2N$-flux as the HEP, PtO_x/WO_3 as the OEP, and IO_3^-/I^- as the redox mediator exhibited twofold greater activity than an analogous system based on $BaTaO_2N$ synthesized without the flux.

Another example reported by Zhang and coworkers is the addition of Mg powder during the nitridation of $YTaO_{4-x}N_y$ from $YTaO_4$.[25] The added Mg increased the N content in the nitridation product and extended the absorption edge toward longer wavelengths. This effect was attributed to Mg functioning as a reducing reagent to weaken the metal–oxygen bond in $YTaO_4$ to facilitate the replacement of O atoms by N atoms. Using Pt/$YTaO_{4-x}N_y$ as the HEP, PtO_x/WO_3 as the OEP, and IO_3^-/I^- as the redox mediator, the authors constructed a Z-scheme system that could split water into H_2 and O_2 under visible light.

The second approach is constructing solid solutions between two different semiconductors to tune the bandgap energy. In 2011, Maeda *et al.* prepared a $BaZrO_3$–$BaTaO_2N$ solid solution by nitriding a mixture of $BaZrO_x$ and $BaTaO_x$.[26,27] Because of the incorporation of the $BaZrO_3$ component, this solid solution had a larger bandgap than pure $BaTaO_2N$ and demonstrated a stronger driving force for the HER and OER. In addition, the defect density in the $BaZrO_3$–$BaTaO_2N$ solid solution decreased because the background absorption beyond the absorption-edge wavelength (650 nm) decreased. After being modified with Pt as a H_2-evolution cocatalyst (HEC), the $BaZrO_3$–$BaTaO_2N$ solid solution exhibited enhanced HER activity. It was applicable to Z-scheme OWS; however, the AQY at 420–440 nm was less than 0.1%. Similarly, $SrZrO_3$ was found to enlarge the bandgap and reduce the defect density of $LaTaON_2$ by forming solid solutions.[28] Compared with pristine $LaTaON_2$, the $LaTaON_2$–$SrZrO_3$ solid solution exhibited enhanced OER activity. Moreover, when coupled with Ru/$SrTiO_3$:Rh in $FeCl_3$ solution, the $LaTaON_2$–$SrZrO_3$ solid solution split water into stoichiometric H_2 and O_2 under visible light *via* a Z-scheme process.

Doping is also a prevalent strategy in the preparation of photocatalysts. The introduction of foreign elements enables control of the optical, particle, and semiconducting properties. For example, doping $BaTaO_2N$ with a moderate amount of Zr was shown to enhance the H_2 evolution of Na–Pt/$BaTaO_2N$.[29] Analysis by transient absorption spectroscopy (TAS) showed that doping with 1 mol% Zr could increase the population of shallowly trapped electrons and that increasing the amount of Zr to 10 mol% reduced both the electron and hole densities. When combined with CoO_x/Au/$BiVO_4$ as the OEP and $[Fe(CN)_6]^{3-}/[Fe(CN)_6]^{4-}$ as the redox mediator, Na–Pt/$BaTaO_2$-N:Zr exhibited an AQY of 1.5% at 420 nm and an STH of 2.2×10^{-2}% in Z-scheme OWS.

Promotion of charge separation and migration

The efficiency of photocatalysis is affected by both carrier recombination and charge separation/migration. The anisotropic nature of some semiconductors, such as $SrTiO_3$ and $BiVO_4$, can provide materials with a sufficient driving force for the separation and transportation of photogenerated electrons and holes toward surface reduction and oxidation sites, respectively.[30,31] The facet-selective loading of cocatalysts onto these materials can substantially reduce the charge recombination probability and improve the charge separation efficiency. As previously mentioned, the difficulty in constructing transition-metal (oxy)nitrides with high crystallinity and anisotropic facet exposure limits the applicability of this strategy. Nevertheless, recent studies have suggested that flux-assisted nitridation can overcome this limitation. Luo *et al.* showed that {100} and {110} facets can be exposed simultaneously on $BaTaO_2N$ when a KCl flux is used.[32] In addition, Pt nanoparticles can be selectively photo-deposited onto the {100} facets. This feature enhanced the charge separation of $BaTaO_2N$, leading to tenfold greater HER activity compared with that of $BaTaO_2N$ with only its {100} facets exposed.[32] This observation suggests that facet-selective cocatalyst loading methods can be applied to transition-metal (oxy)nitrides.

A heterostructure system can promote photoexcited electron and hole transfer in different directions. Such systems are also often effective for forming heterojunctions promoting the functionality of transition-metal (oxy)nitride photocatalysts. Chen *et al.* prepared a $MgTa_2O_{6-x}N_y$/TaON heterostructure *via* the one-pot nitridation of $MgTa_2O_6/Ta_2O_5$ (Fig. 3a).[33] Because the photodeposition of Pt nanoparticles mainly occurred on the TaON surface (Fig. 3b), the authors suggested that photogenerated electrons migrated toward the conduction-band minimum of TaON while holes migrated to the valence-band maximum of $MgTa_2O_{6-x}N_y$. Benefitting from the effective interfacial charge separation and reduced defect density, the AQY for Z-scheme OWS involving $MgTa_2O_{6-x}N_y$/TaON reached 6.8% at 420 nm. This strategy has also been extended to similar bi-(oxy)nitride heterojunctions such as $BaTaO_2N/Ta_3N_5$,[34,35] $BaMg_{1/3}Ta_{2/3}O_{3-x}N_y/Ta_3N_5$,[36] and $CaTaO_2N/Ta_3N_5$.[37] Analyses using Kelvin probe force microscopy (KPFM) and electrochemical impedance spectroscopy (EIS) demonstrated enhanced charge separation in the $BaTaO_2N/Ta_3N_5$ and $CaTaO_2N/Ta_3N_5$ heterojunction systems (Fig. 3c and d) according to the authors of the articles.[34,37]

Cocatalyst design promoting surface redox reactions

The cocatalyst is also an important component of OWS systems. Cocatalysts are expected to promote not only charge separation and transfer but also surface redox reactions. This function will,

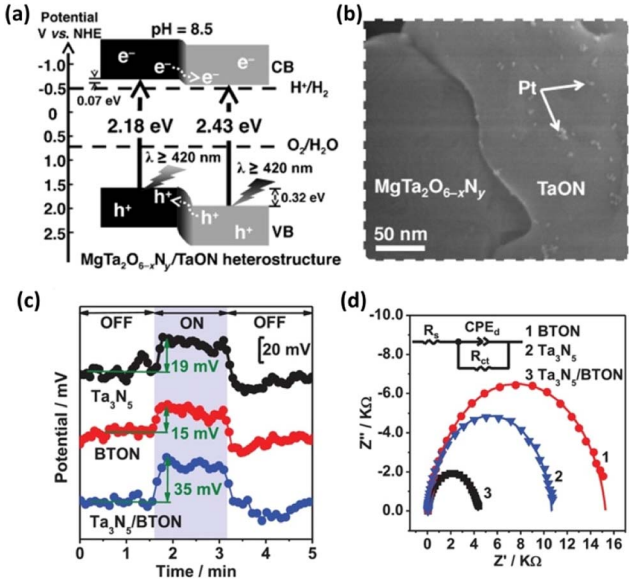

Fig. 3 (a) Estimated band positions for the $MgTa_2O_{6-x}N_y$/TaON heterostructure. (b) Field-emission scanning electron microscopy images of the Pt–$MgTa_2O_{6-x}N_y$/TaON photocatalyst. Adapted with permission from ref. 33. Copyright 2015 Wiley-VCH. (c) Surface potentials of three typical BTON in the dark and under irradiation with 450 nm light. (d) EIS results for three BTON measured at 1.23 V *vs.* the reversible hydrogen electrode (RHE). Adapted with permission from ref. 34. Copyright 2019 Wiley-VCH.

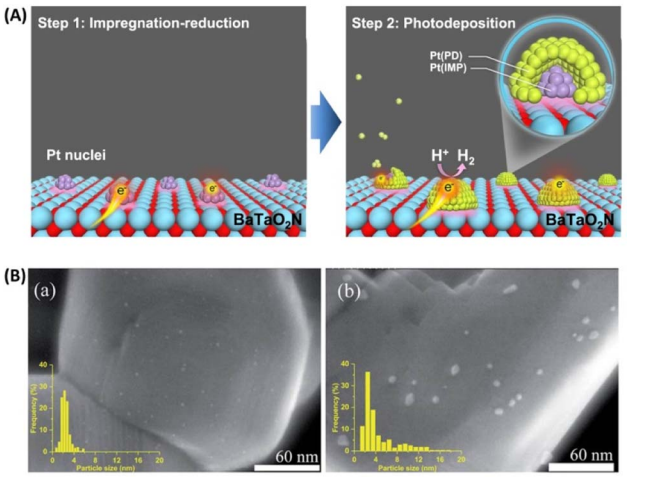

Fig. 4 (A) Schematic of sequential Pt cocatalyst deposition onto $BaTaO_2N$. Adapted with permission from ref. 40. Copyright 2021 Springer Nature. (B) Scanning transmission electron microscopy images and particle size distributions of (a) Na-containing and (b) Na-free Pt/$BaTaO_2N$. Adapted with permission from ref. 41. Copyright 2021 The Royal Society of Chemistry.

in turn, necessitate intimate interfacial contact between semiconductors and cocatalysts *via* a suitable junction. However, (oxy)nitrides might decompose into oxides at high temperatures in air. To avoid the decomposition of (oxy)nitrides during the loading of cocatalysts, Zhang *et al.* devised a method to load CoO_x as an OEC onto (oxy)nitrides under a high-temperature NH_3 flow.[38] Strong interfacial interaction occurred between the Co species and $LaTiO_2N$, without destruction of the oxynitride. The resultant CoO_x/$LaTiO_2N$ exhibited an excellent AQY in the OER (27.1 ± 2.6% at 440 nm).

Concerning the HER, a sequential cocatalyst loading procedure (*i.e.*, impregnation–reduction, followed by photodeposition) was recently developed to modify Ta_3N_5 and $BaTaO_2N$ with highly dispersed and intimately contacted Pt nanoparticles (Fig. 4A).[39,40] The HER activity of the resultant Pt/$BaTaO_2N$ was enhanced almost threefold compared with the case of $BaTaO_2N$ modified with Pt *via* an impregnation–reduction procedure.[40] Z-scheme OWS using Pt/$BaTaO_2N$ as the HEP and PtO_x/WO_3 as the OEP exhibited an AQY of 4.0% at 420 nm and an STH of 0.24%.[40] Moreover, electron transfer from $BaTaO_2N$ to the Pt nanoparticles was verified *via* TAS experiments. The absorption intensity at 5000 cm^{-1} (2000 nm, 0.62 eV) for Pt/$BaTaO_2N$ decayed faster when Pt was loaded *via* a two-step procedure than when it was loaded *via* only a single-step impregnation–reduction procedure or *via* photodeposition. Notably, the HER activity of Pt/$BaTaO_2N$ was well correlated with the OWS activity of the Z-scheme systems, indicating that further improvements in the performance of the HEP based on Pt/$BaTaO_2N$ will improve the OWS activity of this Z-scheme system.[40] Adding a small amount of Na^+ during the impregnation of Pt is another method to fabricate well-dispersed Pt nanoparticles on the surface of $BaTaO_2N$ (Fig. 4B), resulting in Pt/$BaTaO_2N$ with improved HER activity.[41]

In an ideal Z-scheme system, ionic redox mediators can transfer electrons and holes between two different photocatalysts. However, backward reactions involving redox mediators generally suppress the OWS activity because these side reactions are thermodynamically more favorable. Moreover, the activity of Z-scheme OWS systems is, in most cases, highly sensitive to the kinds and concentrations of the redox mediators. As an example, IrO_2/TaON can oxidize water to O_2 in the presence of $AgNO_3$ as a sacrificial electron acceptor; however, it exhibits almost no OER activity in an aqueous $NaIO_3$ solution, likely because of preferential oxidation of the generated I^- ions.[42] To avoid problems arising from reversible redox mediators, solid electron conductors such as reduced graphene oxide (RGO) and Au have been applied to Z-scheme systems involving transition-metal (oxy)nitrides. Z-scheme photocatalyst sheets consisting of $RhCrO_x/ZrO_2/LaMg_{1/3}Ta_{2/3}O_2N$ as the HEP and $BiVO_4$:Mo as the OEP embedded in a Au layer have been reported to split water under visible-light irradiation; however, the STH is still low ($\sim 1 \times 10^{-3}$%).[43] The STH was slightly improved to 3.5×10^{-3}% when RGO was introduced as an additional solid electron conductor into this system; this improvement was attributed to an enhancement in the efficiency of charge transfer between the photocatalytic particles (Fig. 5).[44] Moreover, (oxy)nitrides can be used as the OEP in a Z-scheme sheet system.[45] A photocatalyst sheet based on Ga-doped $La_5Ti_2Cu_{0.9}Ag_{0.1}O_7S_5$ as the HEP and CoO_x/$LaTiO_2N$ as the OEP embedded in a thin Au film split water with an AQY in the order of 10^{-2}% at 420 nm. In this case, CoO_x was suggested to promote not only the OER on $LaTiO_2N$ but also electron transfer from $LaTiO_2N$ to Au.[45]

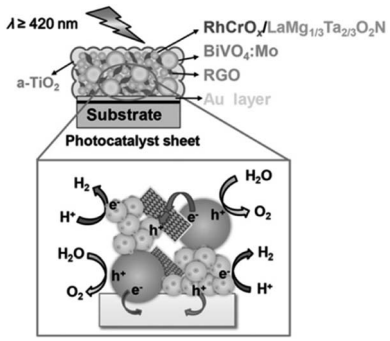

Fig. 5 Schematic of a-TiO_2-coated ($RhCrO_x$/ZrO_2/$LaMg_{1/3}Ta_{2/3}O_2N$)/(Au, RGO)/$BiVO_4$:Mo photocatalyst sheet. Adapted with permission from ref. 44. Copyright 2016 Wiley-VCH.

One-step-excitation OWS systems

Compared with the Z-scheme OWS system, the one-step-excitation OWS reaction is a relatively simpler system that uses only one semiconductor material as a photocatalyst. Nevertheless, because of the rigorous requirements for the one-step-excitation OWS procedure, only a limited number of (oxy)nitrides have achieved OWS *via* such a mode. Herein, we first highlight a typical example that combines band engineering and surface modification to achieve one-step-excitation OWS by using an (oxy)nitride photocatalyst for the first time. We then focus on cases based on a dual-cocatalyst strategy that have recently been widely applied.

Combination of band engineering and surface modification

In 2015, our group reported, for the first time, one-step-excitation OWS under visible light with wavelengths as long as 600 nm using an $LaMg_{1/3}Ta_{2/3}O_2N$ photocatalyst (Fig. 6a).[46] In this case, both band engineering and surface modification were used. Through the formation of solid solutions of two perovskite-type semiconductors ($LaTaON_2$ and $LaMg_{2/3}Ta_{1/3}O_3$), the absorption-edge wavelength of $LaMg_xTa_{1-x}O_{1+3x}N_{2-3x}$ varied from 525 to 640 nm with a decreasing value of x from 0.6 to 0 because of the increase in the O-to-N ratio in conjunction with the substitution of Mg^{2+} for Ta^{5+}. According to theoretical calculations and a photoelectron spectroscopy investigation, the valence-band maximum was shifted toward more positive potentials, leading to an improvement in both the OER and OWS reaction (Fig. 6b).[47] Mg^{2+} was also found to tune the bandgap of $LaMg_xNb_{1-x}O_{1+3x}N_{2-3x}$; the OWS reaction could only be achieved when a suitable amount of Mg^{2+} was present.[48]

Recently, the substitution of Ca^{2+} for La^{3+} in $LaTaO_2N$ was investigated to modulate the band structure and defect concentration *via* the formation of a $(LaTaON_2)_{1-x}(CaTaO_2N)_x$ solid solution.[49] After the optimized $La_{0.1}Ca_{0.9}TaO_{1+y}N_{2-y}$ was decorated with $RhCrO_x$ as a cocatalyst, it exhibited OWS activity, with an AQY of ~0.06% at ~420 nm. In contrast to $La_{0.1}Ca_{0.9}TaO_{1+y}N_{2-y}$, neither $LaTaO_2N$ nor $CaTaO_2N$ showed activity toward the OWS reaction when used as a photocatalyst. Our group reported one-step-excitation OWS using $CaTaO_2N$ modified with $RhCrO_x$; however, the AQY was low (on the order of 10^{-3}% at 440 nm).[50]

The surface of $LaMg_{1/3}Ta_{2/3}O_2N$ was also modified with a nanolayer of amorphous oxyhydroxide (OXH).[46,51] Photodegradation of the (oxy)nitride and the water-formation reaction were both suppressed after the entire $RhCrO_x$/$LaMg_{1/3}Ta_{2/3}O_2N$ surface was coated with a TiOXH layer. Such a deposited OXH nanolayer can function as a molecular sieve, where H_2 and O_2 evolved on the surface of $RhCrO_x$/$LaMg_{1/3}Ta_{2/3}O_2N$ can migrate to the outer phase, whereas migration in the opposite direction is inhibited. As a result, backward reactions involving the O_2 reduction reaction are effectively suppressed. Moreover, compared with $RhCrO_x$/$LaMg_{1/3}Ta_{2/3}O_2N$ coated only with a TiOXH layer, $RhCrO_x$/$LaMg_{1/3}Ta_{2/3}O_2N$ coated with both TiOXH and SiOXH layers showed enhanced OWS activity.[51] We speculated that the double coating layer was more uniform because SiOXH could increase the hydrophilicity. The AQY at 440 ± 30 nm was increased from ~3 × 10^{-2}% to 0.18% by optimization of the nanolayer precursor and deposition procedure.

Strategies based on dual cocatalysts

A dual-cocatalyst strategy is another prevalent method used to realize one-step-excitation OWS reactions.[52–54] Because the surface HER and OER are sluggish, enhancing both the HER

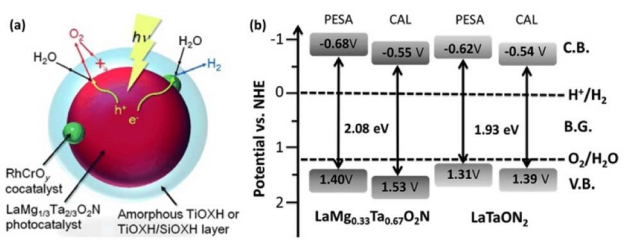

Fig. 6 (a) Schematic of the OWS reaction mechanism on surface-coated $RhCrO_x$/$LaMg_{1/3}Ta_{2/3}O_2N$. Adapted with permission from ref. 46. Copyright 2015 Wiley-VCH. (b) Band levels for $LaMg_xNb_{1-x}O_{1+3x}N_{2-3x}$ (x = 0 and 0.33) estimated by theoretical calculations (CAL) and photoelectron spectroscopy in air (PESA). Adapted with permission from ref. 47. Copyright 2016 The Royal Society of Chemistry.

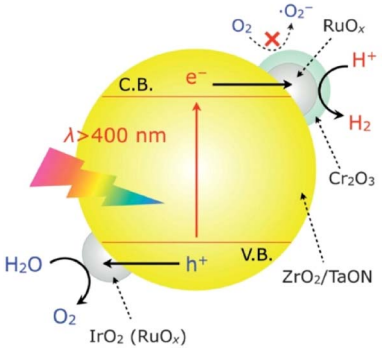

Fig. 7 Schematic of the OWS mechanism on IrO_2/Cr_2O_3/RuO_x/ZrO_2/TaON. Adapted with permission from ref. 55. Copyright 2013 Wiley-VCH.

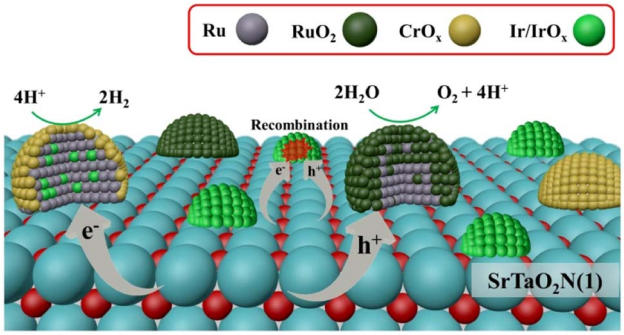

Fig. 8 Schematic of dispersion of cocatalysts and dominant charge transfer processes on the $SrTaO_2N$ surface. Adapted with permission from ref. 57. Copyright 2023 American Chemical Society.

and OER simultaneously is critical, particularly for narrow-bandgap oxynitrides. In this context, the adsorption of colloidal IrO_2 onto the surface of an oxynitride semiconductor surface is a feasible approach. For example, $IrO_2/Cr_2O_3/RuO_x/ZrO_2$/TaON has been reported to split water into H_2 and O_2 in a stoichiometric ratio under visible-light irradiation; however, the AQY was less than 0.1% at 420 nm (Fig. 7).[55] In this system, Cr_2O_3/RuO_x can extract photogenerated electrons from ZrO_2/TaON while IrO_2 provides water oxidation sites that consume photogenerated holes. For comparison, ZrO_2/TaON loaded with only the HEC (*i.e.*, $Cr_2O_3/RuO_x/ZrO_2$/TaON) exhibited relatively lower activity and stability for OWS. Notably, TaON without the ZrO_2 modification could not split water; modifying the surface of TaON with ZrO_2 nanoparticles to suppress the formation of surface defects (Ta^{3+} or Ta^{4+}) was indispensable for realizing OWS. Recently, Zr-doped TaON (TaON:Zr) was fabricated using small, amorphous $Ta_2O_5 \cdot 3.3H_2O$ particles as a precursor.[56] As a result of a substantially reduced particle size by precursor design and a lowered defect density by Zr doping, IrO_2/Cr_2O_3/Ru/TaON:Zr achieved greater AQY (420 nm) and STH values of 0.66% and 9×10^{-3}%, respectively. Similarly, IrO_2/Cr_2O_3/Rh/$BaTaO_2N$:Mg, which features combined dual cocatalyst loading and lower-valent-cation doping, achieved one-step-excitation OWS with an AQY of 0.08% at 420 nm and an STH of 4×10^{-4}%.[14] Notably, $BaTaO_2N$:Mg has the smallest bandgap (~1.9 eV) among the materials that have achieved one-step-excitation OWS.

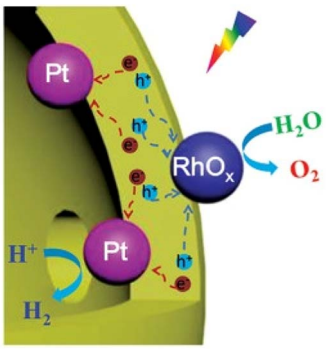

Fig. 9 Schematic of charge separation processes on Pt@$ZnTiO_{3-x}N_y$@RhO_x. Adapted with permission from ref. 59. Copyright 2021 Wiley-VCH.

In addition to the use of colloidal IrO_2, other strategies have been developed to fabricate dual cocatalysts. Recently, bimetallic nanoparticle cocatalysts were loaded onto a $SrTaO_2N$-based photocatalyst using microwave-assisted heating (Fig. 8).[57] Specifically, highly dispersed IrO_2 nanoparticles were deposited through microwave-assisted heating. Subsequent loading of Ru species by impregnation and H_2 reduction produced bimetallic $RuIrO_x$ nanoparticles. The resultant bimetallic nanoparticles were found to effectively extract electrons from semiconductors and accelerate the HER. Coexisting RuO_x served as an OEC. The modified $SrTaO_2N$-based photocatalyst exhibited an STH value of 6.3×10^{-3}% and an AQY (420 $\pm$ 30 nm) of 0.34% in the OWS reaction.[57]

Although the dual-cocatalyst strategy can improve OWS activity, the random deposition of HEC and OEC nanoparticles increases the likelihood of charge recombination and the water-formation reaction. The importance of separating the HEC and

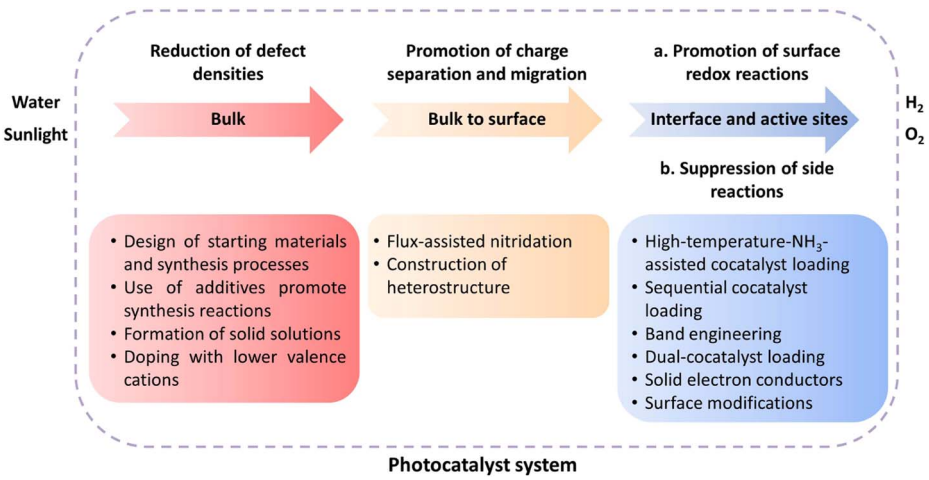

Fig. 10 Summary of challenges and recent strategies.

OEC has been suggested in some earlier studies. For instance, a Ta_3N_5 hollow-sphere photocatalyst whose inner and outer shells were loaded with Pt and IrO_2 or CoO_x, respectively, exhibited enhanced HER and OER activities compared with Ta_3N_5 hollow-sphere particles randomly loaded with the cocatalysts.[58] Xu *et al.* constructed $ZnTiO_{3-x}N_y$ hollow nanospheres using carbon spheres as a template and selectively deposited Pt as the HEC and RhO_x as the OEC onto the inner and outer surfaces, respectively (Fig. 9).[59] Compared with $ZnTiO_{3-x}N_y$ hollow nanospheres with randomly decorated cocatalyst nanoparticles, such a selective deposition method was found to improve the AQE of the one-step-excitation OWS reaction eightfold to 0.22% (420 ± 20 nm) and to increase the STH to 0.02%. The improvement in photocatalytic activity was attributed to the core–shell photocatalyst and the spatial separation of the cocatalysts, both of which can enhance the separation of photogenerated electrons and holes as well as inhibit the backward reaction. The use of hollow-sphere photocatalysts offers opportunities to separate the cocatalyst loading sites. However, a key issue in this approach is the difficulty associated with preparing single-crystal shells. If the photocatalyst shell is polycrystalline, it will contain grain boundaries; thus, charge separation might not be promoted even if cocatalysts are loaded with good spatial separation.

Conclusion and outlook

Over the past decade, numerous transition-metal (oxy)nitride semiconductors capable of driving the OWS reaction *via* the Z-scheme or one-step excitation have been reported. Traditionally, efforts have been devoted to reducing the defect density while suppressing the excessive growth of particles in the development of transition-metal (oxy)nitrides because they often contain defects as a result of harsh nitridation conditions (Fig. 10). To this end, modifications of precursors and refinements of the preparation conditions (*e.g.*, flux-assisted nitridation and aliovalent doping) and post-treatment (*e.g.*, surface modifications) have been applied, partially solving the problem. Additional efforts have been devoted to improving charge separation/migration and surface redox reactions while suppressing side reactions through surface modifications. However, the STH achieved with existing (oxy)nitride photocatalysts falls far short of the goal (>5%). Given the AQY values (<7% for Z-scheme OWS and ≤0.02% for one-step-excitation OWS), only a very small portion of photons are successfully used to split water. Thus, establishing strategies that can enhance charge separation/injection and suppress side reactions is critical.

Much room remains for further improving the synthesis of transition-metal (oxy)nitrides (Fig. 10). Such improvements will remain an important approach to enhancing the OWS activity to reduce the particle size, because smaller particles shorten the charge carrier migration distance and, in principle, lower the probability of recombination in the bulk of the material if the crystallinity and the defect density are not deteriorated. One approach to balancing small particle size and high crystallinity is to synthesize one-dimensional (rod-like) or two-dimensional (sheet-like) transition-metal (oxy)nitride single-crystal nanoparticles and exploit their anisotropic crystal structures. For example, single-crystalline Ta_3N_5 nanorods generated directly on the edges of $KTaO_3$ particles have been reported to split water without any sacrificial agent, whereas bulk Ta_3N_5 was inactive.[60] In addition, given the profound effect of starting materials on the particle and material properties of transition-metal (oxy)nitrides obtained by thermal nitridation, a survey of starting materials and detailed examinations of the nitridation process might provide clues for dramatically improving the synthesis of photocatalyst materials.

Another promising strategy is the site-selective loading of cocatalysts, which has been applied to oxide photocatalysts, resulting in a substantial improvement in their OWS activity. However, this strategy has not been successfully applied to transition-metal (oxy)nitrides. A major challenge is how to prepare (oxy)nitrides with high crystallinity and exposed anisotropic facets.

Regarding the Z-scheme OWS system, when (oxy)nitrides are used as either the HEP or OEP, oxide photocatalysts are used as their counterpart in most cases. Utilizing a wider range of visible light necessitates the development of a Z-scheme OWS system solely involving (oxy)nitride photocatalysts with an absorption-edge wavelength greater than 600 nm. To this end, the design of (oxy)nitrides that can drive the HER and/or OER efficiently and with high selectivity (*i.e.*, without promoting reverse or side reactions) is also desirable. The photocatalyst sheet system based on HEPs and OEPs fixed with conductive materials is a particularly promising approach to realizing efficient Z-scheme OWS, given the relatively high STH and potential scalability demonstrated for some oxide photocatalysts. An STH beyond 1% has been achieved by a $SrTiO_3$:La,Rh/C/$BiVO_4$:Mo photocatalyst sheet even under ambient pressure.[61] However, the highest STH achieved with photocatalyst sheets based on transition-metal (oxy)nitrides is 3.5×10^{-3}% for ($RhCrO_x$/ZrO_2/$LaMg_{1/3}Ta_{2/3}O_2N$)/(Au,RGO)/$BiVO_4$:Mo.[44] A better understanding of the low activity is needed, and the photocatalytic activity should be further improved through appropriate design. Research into solid-state electron conductors is important but is still in progress and immature.[15,62] A photovoltaic-electrochemical (PV-EC) solar hydrogen production system is also a choice for transition-metal (oxy)nitride semiconductors because significant progress has been achieved in such systems.[63] However, approaches to scale up the system and reduce manufacturing costs should also be identified.

Overall, transition-metal (oxy)nitrides constitute a promising group of materials for OWS catalysts because their absorption-edge wavelength is sufficiently long to meet the STH target and their band positions can be controlled. We hope this perspective will facilitate progress in this field and bridge the gap between what researchers have achieved and what society needs for practical solar hydrogen production *via* photocatalytic water splitting.

Author contributions

Kaihong Chen: conceptualization, writing original draft, writing review & editing; Jiadong Xiao: conceptualization, writing

review & editing; Takashi Hisatomi: conceptualization, writing review & editing; Kazunari Domen: conceptualization, funding acquisition, writing review & editing.

Conflicts of interest

The authors declare no competing financial interest.

Acknowledgements

This work was financially supported by the Artificial Photosynthesis Project of the New Energy and Industrial Technology Development Organization (NEDO) and JST-PRESTO (JPMJPR20T9). K. C. acknowledges support from the Japanese Society for Promotion of Sciences (JSPS, grand no. P21038) for Overseas Researchers and the National Natural Science Foundation of China (grant no. 22005154).

References

1 G. Segev, J. Kibsgaard, C. Hahn, Z. J. Xu, W. H. Cheng, T. G. Deutsch, C. X. Xiang, J. Z. Zhang, L. Hammarstrom, D. G. Nocera, A. Z. Weber, P. Agbo, T. Hisatomi, F. E. Osterloh, K. Domen, F. F. Abdi, S. Haussener, D. J. Miller, S. Ardo, P. C. McIntyre, T. Hannappel, S. Hu, H. Atwater, J. M. Gregoire, M. Z. Ertem, I. D. Sharp, K. S. Choi, J. S. Lee, O. Ishitani, J. W. Ager, R. R. Prabhakar, A. T. Bell, S. W. Boettcher, K. Vincent, K. Takanabe, V. Artero, R. Napier, B. Roldan Cuenya, M. T. M. Koper, R. Van de Krol and F. Houle, *J. Phys. D: Appl. Phys.*, 2022, **55**, 323003.

2 T. Takata, J. Z. Jiang, Y. Sakata, M. Nakabayashi, N. Shibata, V. Nandal, K. Seki, T. Hisatomi and K. Domen, *Nature*, 2020, **581**, 411–414.

3 T. Hisatomi and K. Domen, *Nat. Catal.*, 2019, **2**, 387–399.

4 J. D. Xiao, T. Hisatomi and K. Domen, *Acc. Chem. Res.*, 2023, **56**, 878–888.

5 X. P. Tao, Y. Zhao, S. Y. Wang, C. Li and R. G. Li, *Chem. Soc. Rev.*, 2022, **51**, 10120–10122.

6 M. Xiao, S. Wang, S. Thaweesak, B. Luo and L. Wang, *Engineering*, 2017, **3**, 365–378.

7 Y. F. Bao, C. Li, K. Domen and F. X. Zhang, *Acc. Mater. Res.*, 2022, **3**, 449–460.

8 B. B. Dong, J. Y. Cui, Y. Qi and F. X. Zhang, *Adv. Mater.*, 2021, **33**, 2004697.

9 S. J. Jiang, Y. X. Liu and J. Xu, *Mater. Adv.*, 2021, **2**, 1190–1203.

10 T. Takata, C. S. Pan and K. Domen, *Sci. Technol. Adv. Mater.*, 2015, **16**, 033506.

11 Q. Wang and K. Domen, *Chem. Rev.*, 2020, **120**, 919–985.

12 W. Wang, M. O. Tadé and Z. Shao, *Prog. Mater. Sci.*, 2018, **92**, 33–63.

13 S. Du, J. Lian and F. Zhang, *Trans. Tianjin Univ.*, 2023, **28**, 33–52.

14 H. Li, J. Xiao, J. J. M. Vequizo, T. Hisatomi, M. Nakabayashi, Z. Pan, N. Shibata, A. Yamakata, T. Takata and K. Domen, *ACS Catal.*, 2022, **12**, 10179–10185.

15 H. Nishiyama, T. Yamada, M. Nakabayashi, Y. Maehara, M. Yamaguchi, Y. Kuromiya, Y. Nagatsuma, H. Tokudome, S. Akiyama, T. Watanabe, R. Narushima, S. Okunaka, N. Shibata, T. Takata, T. Hisatomi and K. Domen, *Nature*, 2021, **598**, 304–307.

16 Y. W. Ma, L. H. Lin, T. Takata, T. Hisatomi and K. Domen, *Phys. Chem. Chem. Phys.*, 2023, **25**, 6586–6601.

17 T. Hisatomi, K. Takanabe and K. Domen, *Catal. Lett.*, 2015, **145**, 95–108.

18 T. Hisatomi and K. Domen, *Next Energy*, 2023, **1**, 100006.

19 K. Maeda, *ACS Catal.*, 2013, **3**, 1486–1503.

20 Y. O. Wang, H. Suzuki, J. J. Xie, O. Tomita, D. J. Martin, M. Higashi, D. Kong, R. Abe and J. W. Tang, *Chem. Rev.*, 2018, **118**, 5201–5241.

21 S. Chang, J. Yu, R. Wang, Q. Fu and X. Xu, *ACS Nano*, 2021, **15**, 18153–18162.

22 L. Yang, Q. Fu, L. Wang, J. Yu and X. Xu, *Appl. Catal., B*, 2022, **304**, 120934.

23 L. Yang, J. X. Yu, Q. Y. Fu, L. L. Kong and X. X. Xu, *Nano Energy*, 2022, **95**, 107059.

24 B. Dong, Y. Qi, J. Cui, B. Liu, F. Xiong, X. Jiang, Z. Li, Y. Xiao, F. Zhang and C. Li, *Dalton Trans.*, 2017, **46**, 10707–10713.

25 H. Zou, Y. Bao, S. Du, X. Xin, Y. Qi, G. Shao and F. Zhang, *Chem.–Asian J.*, 2023, **18**, e202300145.

26 T. Matoba, K. Maeda and K. Domen, *Chem.–Eur. J.*, 2011, **17**, 14731–14735.

27 K. Maeda, D. Lu and K. Domen, *ACS Catal.*, 2013, **3**, 1026–1033.

28 R. Wang, Y. Wang, S. Chang, S. Jin, Y. Shao and X. Xu, *J. Catal.*, 2020, **390**, 57–66.

29 H. Li, J. J. M. Vequizo, T. Hisatomi, M. Nakabayashi, J. Xiao, X. Tao, Z. Pan, W. Li, S. Chen, Z. Wang, N. Shibata, A. Yamakata, T. Takata and K. Domen, *EES Catal.*, 2023, **1**, 26–35.

30 L. C. Mu, Y. Zhao, A. L. Li, S. Y. Wang, Z. L. Wang, J. X. Yang, Y. Wang, T. F. Liu, R. T. Chen, J. Zhu, F. T. Fan, R. G. Li and C. Li, *Energy Environ. Sci.*, 2016, **9**, 2463–2469.

31 R. G. Li, F. X. Zhang, D. G. Wang, J. X. Yang, M. R. Li, J. Zhu, X. Zhou, H. X. Han and C. Li, *Nat. Commun.*, 2013, **4**, 1432.

32 Y. Luo, S. Suzuki, Z. Wang, K. Yubuta, J. J. M. Vequizo, A. Yamakata, H. Shiiba, T. Hisatomi, K. Domen and K. Teshima, *ACS Appl. Mater. Interfaces*, 2019, **11**, 22264–22271.

33 S. Chen, Y. Qi, T. Hisatomi, Q. Ding, T. Asai, Z. Li, S. S. Ma, F. Zhang, K. Domen and C. Li, *Angew. Chem., Int. Ed.*, 2015, **54**, 8498–8501.

34 B. Dong, J. Cui, Y. Gao, Y. Qi, F. Zhang and C. Li, *Adv. Mater.*, 2019, **31**, e1808185.

35 Y. Qi, S. Chen, M. Li, Q. Ding, Z. Li, J. Cui, B. Dong, F. Zhang and C. Li, *Chem. Sci.*, 2017, **8**, 437–443.

36 J. Cui, Y. Qi, B. Dong, L. Mu, Q. Ding, G. Liu, M. Jia, F. Zhang and C. Li, *Appl. Catal., B*, 2019, **241**, 1–7.

37 Y. Luo, H. Li, Y. Luo, Z. Li, Y. Qi, F. Zhang and C. Li, *J. Energy Chem.*, 2022, **67**, 27–33.

38 F. Zhang, A. Yamakata, K. Maeda, Y. Moriya, T. Takata, J. Kubota, K. Teshima, S. Oishi and K. Domen, *J. Am. Chem. Soc.*, 2012, **134**, 8348–8351.

39 J. Lian, D. Li, Y. Qi, N. Yang, R. Zhang, T. Xie, N. Guan, L. Li and F. Zhang, *J. Energy Chem.*, 2021, **55**, 444–448.
40 Z. Wang, Y. Luo, T. Hisatomi, J. J. M. Vequizo, S. Suzuki, S. Chen, M. Nakabayashi, L. Lin, Z. Pan, N. Kariya, A. Yamakata, N. Shibata, T. Takata, K. Teshima and K. Domen, *Nat. Commun.*, 2021, **12**, 1005.
41 H. Li, D. Lu, S. Chen, T. Hisatomi, J. J. M. Vequizo, J. Xiao, Z. Wang, L. Lin, Q. Xiao, Y. Sun, Y. Miseki, K. Sayama, A. Yamakata, T. Takata and K. Domen, *J. Mater. Chem. A*, 2021, **9**, 13851–13854.
42 M. Higashi, R. Abe, A. Ishikawa, T. Takata, B. Ohtani and K. Domen, *Chem. Lett.*, 2008, **37**, 138–139.
43 Z. Pan, T. Hisatomi, Q. Wang, S. Chen, M. Nakabayashi, N. Shibata, C. Pan, T. Takata, M. Katayama, T. Minegishi, A. Kudo and K. Domen, *ACS Catal.*, 2016, **6**, 7188–7196.
44 Z. Pan, T. Hisatomi, Q. Wang, S. Chen, A. Iwase, M. Nakabayashi, N. Shibata, T. Takata, M. Katayama, T. Minegishi, A. Kudo and K. Domen, *Adv. Funct. Mater.*, 2016, **26**, 7011–7019.
45 T. Hisatomi, T. Yamamoto, Q. Wang, T. Nakanishi, T. Higashi, M. Katayama, T. Minegishi and K. Domen, *Catal. Sci. Technol.*, 2018, **8**, 3918–3925.
46 C. Pan, T. Takata, M. Nakabayashi, T. Matsumoto, N. Shibata, Y. Ikuhara and K. Domen, *Angew. Chem., Int. Ed.*, 2015, **54**, 2955–2959.
47 C. Pan, T. Takata, K. Kumamoto, S. S. Khine Ma, K. Ueda, T. Minegishi, M. Nakabayashi, T. Matsumoto, N. Shibata, Y. Ikuhara and K. Domen, *J. Mater. Chem. A*, 2016, **4**, 4544–4552.
48 J. Seo, D. Ishizuka, T. Hisatomi, T. Takata and K. Domen, *J. Mater. Chem. A*, 2021, **9**, 8655–8662.
49 Y. Wang, Y. Kang, H. Zhu, G. Liu, J. T. S. Irvine and X. Xu, *Adv. Sci.*, 2021, **8**, 2003343.
50 J. Xu, C. Pan, T. Takata and K. Domen, *Chem. Commun.*, 2015, **51**, 7191–7194.
51 C. Pan, T. Takata and K. Domen, *Chem.–Eur. J.*, 2016, **22**, 1854–1862.
52 K. Maeda, A. K. Xiong, T. Yoshinaga, T. Ikeda, N. Sakamoto, T. Hisatomi, M. Takashima, D. L. Lu, M. Kanehara, T. Setoyama, T. Teranishi and K. Domen, *Angew. Chem., Int. Ed.*, 2010, **49**, 4096–4099.
53 Q. Wang, M. Nakabayashi, T. Hisatomi, S. Sun, S. Akiyama, Z. Wang, Z. H. Pan, X. Xiao, T. Watanabe, T. Yamada, N. Shibata, T. Takata and K. Domen, *Nat. Mater.*, 2019, **18**, 827–832.
54 M. Liu, G. Zhang, X. Liang, Z. Pan, D. Zheng, S. Wang, Z. Yu, Y. Hou and X. Wang, *Angew. Chem., Int. Ed.*, 2023, DOI: **10.1002/anie.202304694**.
55 K. Maeda, D. Lu and K. Domen, *Chem.–Eur. J.*, 2013, **19**, 4986–4991.
56 J. Xiao, S. Nishimae, J. J. M. Vequizo, M. Nakabayashi, T. Hisatomi, H. Li, L. Lin, N. Shibata, A. Yamakata, Y. Inoue and K. Domen, *Angew. Chem., Int. Ed.*, 2022, **61**, e202116573.
57 K. Chen, J. Xiao, J. J. M. Vequizo, T. Hisatomi, Y. Ma, M. Nakabayashi, T. Takata, A. Yamakata, N. Shibata and K. Domen, *J. Am. Chem. Soc.*, 2023, **145**, 3839–3843.
58 D. Wang, T. Hisatomi, T. Takata, C. Pan, M. Katayama, J. Kubota and K. Domen, *Angew. Chem., Int. Ed.*, 2013, **52**, 11252–11256.
59 S. Wei, S. Chang, J. Qian and X. Xu, *Small*, 2021, **17**, e2100084.
60 Z. Wang, Y. Inoue, T. Hisatomi, R. Ishikawa, Q. Wang, T. Takata, S. Chen, N. Shibata, Y. Ikuhara and K. Domen, *Nat. Catal.*, 2018, **1**, 756–763.
61 Q. Wang, T. Hisatomi, Y. Suzuki, Z. Pan, J. Seo, M. Katayama, T. Minegishi, H. Nishiyama, T. Takata, K. Seki, A. Kudo, T. Yamada and K. Domen, *J. Am. Chem. Soc.*, 2017, **139**, 1675–1683.
62 T. Hisatomi and K. Domen, *Curr. Opin. Electrochem.*, 2017, **2**, 148–154.
63 W. Yang, R. R. Prabhakar, J. Tan, S. D. Tilley and J. Moon, *Chem. Soc. Rev.*, 2019, **48**, 1908–1971.